Molecular Psychiatry
https://doi.org/10.1038/s41380-021-01119-9

ARTICLE

Transcription factor 4 controls positioning of cortical projection neurons through regulation of cell adhesion

Yandong Zhang[1] · Zheping Cai[1] · Guanglei Hu[1] · Songhui Hu[1] · Yafei Wang[1] · Na Li[1] · Saiyong Chen[1] · Qiong Liu[1] · Lanhui Zeng[1] · Tianxiang Tang[1] · Yilan Zhang[1] · Lei Xiao[1] · Yu Gu[1] · Yunli Xie[1]

Received: 1 September 2020 / Revised: 2 April 2021 / Accepted: 13 April 2021

Abstract

The establishment of neural circuits depends on precise neuronal positioning in the cortex, which occurs via a tightly coordinated process of neuronal differentiation, migration, and terminal localization. Deficits in this process have been implicated in several psychiatric disorders. Here, we show that the transcription factor Tcf4 controls neuronal positioning during brain development. Tcf4-deficient neurons become mispositioned in clusters when their migration to the cortical plate is complete. We reveal that Tcf4 regulates the expression of cell adhesion molecules to control neuronal positioning. Furthermore, through in vivo extracellular electrophysiology, we show that neuronal functions are disrupted after the loss of Tcf4. TCF4 mutations are strongly associated with schizophrenia and cause Pitt-Hopkins syndrome, which is characterized by severe intellectual disability. Thus, our results not only reveal the importance of neuronal positioning in brain development but also provide new insights into the potential mechanisms underlying neurological defects linked to TCF4 mutations.

Introduction

The establishment of neuronal connections in the mammalian cortex requires precise neuronal positioning, which is tightly controlled during brain development. During cortical development, projection neurons are generated from radial glial progenitors (RGPs) of the dorsal ventricular zone (VZ) [1] and migrate radially along with the basal processes of RGPs toward the cortical plate (CP). During migration, differentiating neurons transiently detach from the basal processes of RGPs and become multipolar within the intermediate zone (IZ) of the cortex prior to the acquisition of bipolar morphology while entering the CP [2, 3]. Upon reaching the CP, migrating neurons enter a "terminal translocation" mode, a radial glial-independent process, to migrate to their final destination [4]. At approximately embryonic day 17.5 (E17.5), shortly before birth, neurogenesis ends and neuronal migration concludes [5, 6]. Precise positioning of neurons in the CP is essential for the establishment of the highly organized six-layered cortical structure, which is fundamental for higher brain functions [7]. Disruptions of any process, including final positioning, during neuronal migration, contribute to the etiology of many neurodevelopmental disorders [8, 9]. Thus, an understanding of the signaling cascades responsible for the regulation of neuronal positioning is essential for defining pathogenic mechanisms.

Neuronal migration along the basal processes of RGPs is tightly regulated by various molecular pathways. In particular, the interaction between RGPs and neurons mediated by cell adhesion plays important role in regulating neuronal migration toward the CP [10, 11]. Suppression of cell–cell adhesion molecules disrupts the attachment of migrating neurons to the basal processes of RGPs, which leads to neuronal migration defects [12–14]. In addition, the Reelin pathway plays an instructive role during neuronal migration to establish the six-layered cortex in a birthdate-dependent manner [7, 15, 16]. However, the molecular mechanisms underlying precise neuronal positioning when neuronal migration is complete remain unclear.

Supplementary information The online version contains supplementary material available at https://doi.org/10.1038/s41380-021-01119-9.

✉ Yunli Xie
Yunli.xie@fudan.edu.cn

[1] Department of Anesthesia, State Key Laboratory of Medical Neurobiology and MOE Frontiers Center for Brain Science, Institutes of Brain Science, and Zhongshan Hospital, Fudan University, Shanghai, China

Published online: 07 May 2021

Tcf4 (also known as E2-2 and ITF2), a basic helix-loop-helix (bHLH) transcription factor, is highly expressed in the nervous system [17, 18]. TCF4 mutations have been linked to Pitt-Hopkins syndrome, a rare neurodevelopmental disorder characterized by severe intellectual disability, speech limitation, motor delay, and visual impairments [18–20]. In addition, single nucleotide polymorphisms in the introns of TCF4 have been associated with schizophrenia [21, 22]. Impairment of Tcf4 function leads to deficits in spatial learning and social activity in adult mice [23, 24]. However, the roles of TCF4 in the developing brain are largely unknown. Here we conditionally inactivated Tcf4 during brain development in mice and found that Tcf4 is essential for neuronal positioning. While Tcf4-deficient neurons migrated normally to the CP during embryonic stages, unexpectedly, they became mispositioned into clusters postnatally when migration was complete. Furthermore, we identified the cell adhesion molecule fibronectin 1 (Fn1) as a key target of Tcf4 in regulating neuronal positioning and found that loss of Tcf4 results in neuronal function deficiency. These findings reveal that the transcriptional regulation of cell adhesion is essential for precise neuronal positioning, which in turn may play a crucial role in circuit function. Therefore, these data provide new insights into potential mechanisms underlying neurological defects linked to TCF4 mutations.

Results

Tcf4 is required for the positioning of pyramidal neurons

Tcf4 is highly expressed in the neocortex and hippocampus during brain development in both neural progenitors and neurons (Supplementary Fig. S1a, b) [17, 24]. The expression of Tcf4 was dynamically regulated during neural development. At the peak of neurogenesis around E14.5, *Tcf4* was expressed in neural progenitors of the VZ and migrating neurons of the IZ (Supplementary Fig. S1c). Interestingly, in the late stage of neurogenesis (E17.5), *Tcf4* expression was downregulated in the migrating neurons in the IZ with an increase in expression in neurons in the CP (Supplementary Fig. S1d). The expression of *Tcf4* in neurons in the CP persisted in the postnatal stages after neuronal migration was complete (Supplementary Fig. S1e–g). The increased expression of Tcf4 in neurons suggests its potential roles in neuronal development.

We then examined the potential functions of Tcf4 in neuronal development by conditional inactivation of Tcf4 in the developing neocortex through Emx1Cre mediated recombination in RGPs and their neuronal progeny [25]. When analyzing the brains of $Tcf4^{f/f}$; Emx1Cre mice (Tcf4 cKO) at postnatal day 7 (P7), we observed that neurons were not positioned properly and formed clusters in the superficial cortical layers which appeared in nearly all brain regions without an obvious pattern (Fig. 1a, b and Supplementary Fig. S2). To reveal the identity of these mispositioned neurons, we stained sections for Satb2, a marker for superficial layer neurons. We found that neurons within the clusters were positive for Satb2 in Tcf4 cKO brains, indicating their superficial neuronal identity (Fig. 1c, d). Distance-based clustering analysis showed that these Satb2-positive neurons were highly clustered in Tcf4 cKO cortices (Fig. 1e, f). Furthermore, we found that neurons within the clusters in Tcf4 cKO brains were also positive for Brn2 and Bhlhb5, markers expressed in superficial layer neurons [26, 27] (Supplementary Fig. S3a, b). To analyze the distribution of Satb2-positive neurons in detail, we quantified the distance from these neurons to the pial basal membrane. In contrast to neurons in wild-type (WT) brains, Satb2-positive neurons in Tcf4 cKO brains often extended to the marginal zone and were close to the pial basal membrane (Fig. 1h). When RGPs were labeled with green fluorescent protein (GFP) through *in utero* electroporation, we found that these late-born neurons were located in clusters and were positive for Satb2 when analyzed at P7 in Tcf4 cKO brains (Fig. 1g, i, j). Conditional removal of Tcf4 did not produce gross defects in neural progenitor proliferation and differentiation (Supplementary Fig. S3c–f). Compared to WT brains, the number of Satb2-positive neurons in Tcf4 cKO brains was reduced (Supplementary Fig. S3g, h). However, we did not detect a significant number of apoptotic neurons at various developmental stages by examining the expression of cleaved caspase 3 in Tcf4 cKO brains (Supplementary Fig. S4) although we could not exclude the immediate clearance of dead cells. To determine whether deep-layer neurons were also affected in Tcf4 cKO brains, we stained the sections for Ctip2, a marker for deep-layer neurons [6]. We found that loss of Tcf4 did not alter the differentiation of Ctip2-positive neurons (Supplementary Fig. S3g, i). The width of the Ctip2-positive neuronal layer became wider and the density of Ctip2-positive neurons was reduced, while the total number of Ctip2-positive neurons remained unchanged in this layer (Supplementary Fig. S3j–l). During cortical development, inhibitory interneurons generated from the medial and caudal ganglionic eminences (MGE and CGE, respectively) follow the position of their pyramidal counterparts in the cortex [28]. To examine whether the distribution of interneurons was altered, we stained the sections for Sox6 and Sp8, markers for cortical inhibitory interneurons derived from the MGE and the CGE respectively. We found that cortical interneurons existed in the clusters of Tcf4-deficient cortices with their excitatory counterparts; however, the total number and the distribution of Sp8-positive and Sox6-positive neurons in different cortical layers were not altered

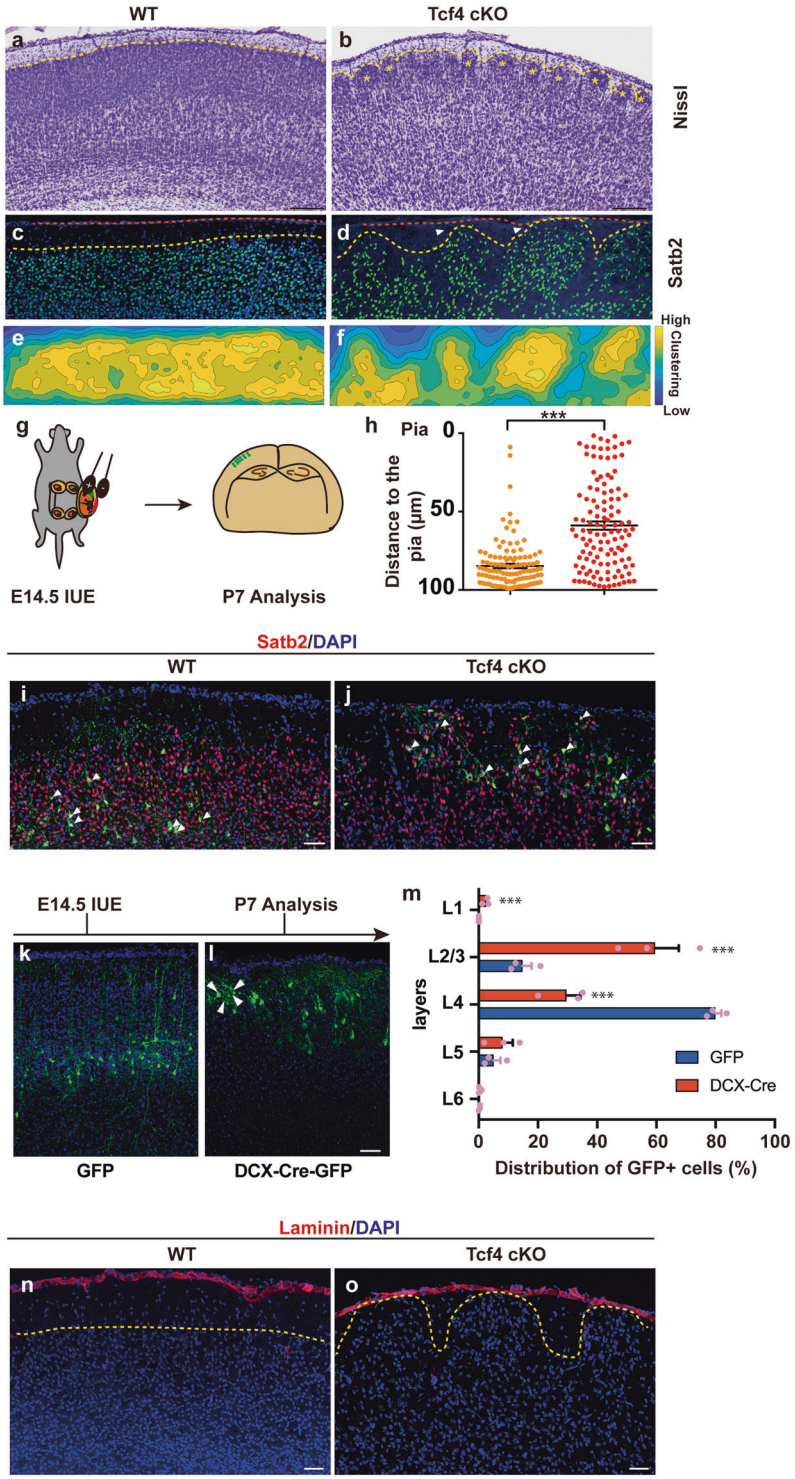

(Supplementary Fig. S5). To further demonstrate that depletion of Tcf4 in neurons can lead to their mispositioning, we electroporated plasmids expressing Cre in neurons driven by the doublecortin (DCX) promoter into RGPs at E14.5. At P7, we found that Tcf4-deficient neurons were positioned close to the pial membrane and clustered (Fig. 1k–m), suggesting a neuronal role of Tcf4 in regulating their positioning. Taken together, these data demonstrate that loss of Tcf4 leads to the mispositioning of cortical neurons.

Disruption of the basal membrane in the developing neocortex results in neuronal ectopias, which are caused

◀ **Fig. 1 Tcf4 is required for neuronal positioning. a, b** Nissl staining of brain sections from WT (**a**) and Tcf4 cKO (**b**) animals. The yellow dashed line indicates the border of upper-layer neurons. Asterisks indicate neuronal clusters. Scale bar: 200 µm. **c**, **d** Representative images of WT (**c**) and Tcf4 cKO (**d**) brain sections stained for Satb2. The red dashed line indicates the pia and the yellow dashed line indicates the border of upper-layer neurons. Arrowheads indicate that neurons of Tcf4 cKO brains are located close to the pia. **e**, **f** Distance-based clustering analysis shows that Tcf4-deficient neurons are highly clustered in Tcf4 cKO brains (**f**) compared to WT brains (**e**). **g** Schematic of *in utero* electroporation approach. **h** Quantification of the distance between the pia and the position of Satb2-positive neurons. Student's *t*-test, $***p < 0.001$, Error bars show mean ± SEM. At least three brains from each phenotype were analyzed. **i**, **j** Immunostaining of both WT (**i**) and Tcf4 cKO (**j**) brain sections for Satb2 and GFP. Arrowheads indicate neurons positive for Satb2 and GFP. Scale bar: 50 µm. **k**, **l** Representative images of brains electroporated with plasmids expressing GFP (**k**) or Cre-GFP driven by the Dcx-promoter (**l**). **m** Quantification of neuronal distribution. $***p < 0.001$, Error bars show mean ± SEM. Student *t*-test was performed to compare two groups, At least three brains were analyzed from each genotype. Scale bar: 50 µm. **n**, **o** The basal membrane revealed by the laminin staining (red) is intact in both WT (**n**) and Tcf4 cKO (**o**) brains. Yellow dashed line indicates the border of neuronal clusters in Tcf4 cKO brains (**o**) and of the upper-layer neurons in WT brains (**n**). Scale bar: 50 µm.

by over migration of neurons beyond the basal membrane, a typical phenotype observed in cobblestone lissencephaly [29]. In contrast, we observed that the basal membrane in Tcf4 cKO brains was intact in both embryonic and postnatal stages (Fig. 1n, o and Supplementary Fig. S6a). After differentiation, neurons migrate radially along with radial glial basal processes towards the CP. By examining the expression of Nestin, a marker for filaments of RGPs, we found that the basal processes were not disrupted upon the loss of Tcf4 (Supplementary Fig. S6a). Furthermore, we labeled the basal processes of RGPs in both WT and Tcf4 cKO brains with a lipophilic tracer, DiI (Supplementary Fig. S6b). After tracing the basal processes, we found that the projection of basal processes of RGPs was normal in Tcf4 cKO brains compared to that of WT brains (Supplementary Fig. S6c–e), suggesting that the phenotype we observed in Tcf4 cKO brains is not due to abnormal basal processes of RGCs and is distinct from cobblestone lissencephaly. Collectively, these data suggest that Tcf4 is required for proper neuronal positioning.

Tcf4 loss leads to neuronal mispositioning in the early postnatal stage

To investigate whether neuronal mispositioning occurs during the embryonic stage when neurons migrate to the CP or postnatally after neuronal migration is complete in Tcf4 cKO brains, we examined the neuronal distribution at both E17.5, when neurogenesis was complete, and P7, when neurons had already reached their destination in the CP. We found that neuronal clustering was not obvious during embryonic development in Tcf4 cKO brains, with a few cells occasionally entering the marginal zone (Supplementary Fig. S7a, b). However, distinct neuronal clusters became visible at P7 when neuronal migration was complete (Supplementary Fig. S7c, d). To further confirm that the neuronal distribution was normal at the end of neurogenesis, we labeled RGPs via *in utero* electroporation at E14.5 and analyzed cluster formation at P0. We found that the distribution of GFP-positive neurons was normal in Tcf4 cKO brains compared to WT brains (Supplementary Fig. 7e–h), which was distinct from the neuronal organization observed at P7 (Fig. 1i, j). Taken together, these data suggest that Tcf4 is required for neuronal positioning during the early postnatal stages when neuron migration is complete.

Migration of Tcf4-deficient neurons during embryonic stages is largely unaffected

To examine whether neuronal mispositioning was due to abnormal migration towards the CP after neuron differentiation, we first labeled RGPs with GFP in WT and Tcf4 cKO brains at E14.5 through *in utero* electroporation and analyzed the progeny 3 days later (Fig. 2a–d). When analyzing the distribution of differentiated neurons, we found that neurons migrated normally to the CP in both WT and Tcf4 cKO brains (Fig. 2a–c). The transition from multipolar to bipolar morphology is a hallmark of migrating neurons and is essential for neuronal migration [30]. We found no obvious defects in the morphological transition upon Tcf4 depletion (Fig. 2d). These data indicate that neuronal migration is not affected in Tcf4 cKO brains. This is consistent with a recent study that used *in utero* electroporation to show that neuronal migration was not affected when Tcf4 was acutely knocked down via RNA interference [31]. To further confirm this observation, we performed time-lapse imaging after *in utero* electroporation (Fig. 2e). We found that both WT and Tcf4-deficient neurons migrated basally to the CP with a largely normal migration behavior (Fig. 2f–i). By analyzing the migration speed of these neurons, we found that neurons in both WT and Tcf4 cKO brains migrated similarly before they reached the pia, while Tcf4-deficient neurons migrated at a higher speed within the CP (Fig. 2j), which may explain that the marginal zone in Tcf4 cKO brains extended basally towards the CP. Indeed, we observed that some Tcf4-deficient neurons migrated tangentially while WT neurons remained stationary when they reached the pia (Fig. 2i, arrowheads). Taken together, these data demonstrate that neuronal migration during early embryonic brain development is largely unaffected by the loss of Tcf4.

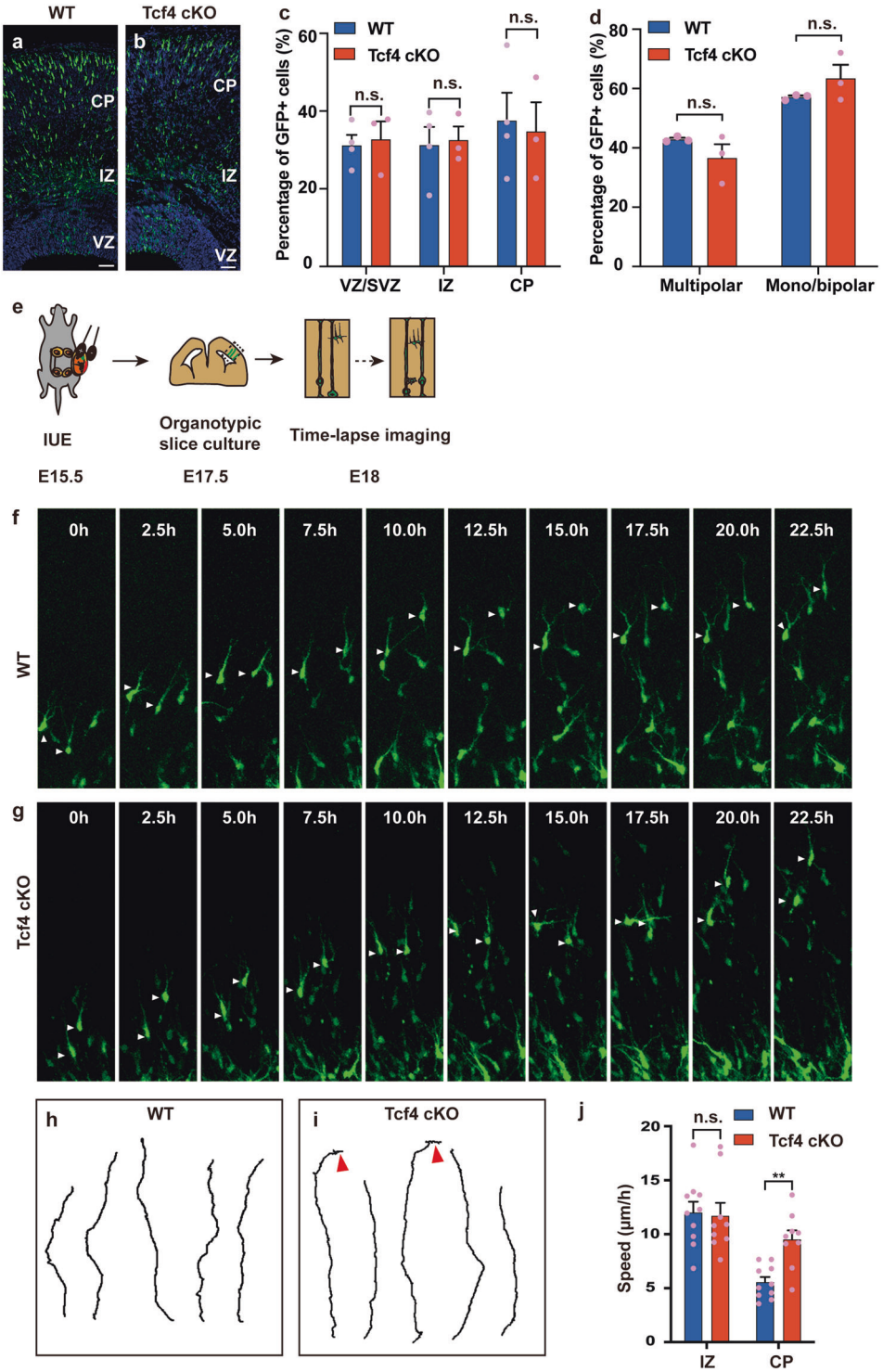

Fig. 2 Tcf4-deficient neurons migrate to the cortical plate. **a**, **b** Representative images for IUE experiments. Constructs expressing GFP were electroporated at E14.5 and brains were analyzed at E17.5 from WT (**a**) and Tcf4 cKO (**b**) mice. Scale bar: 50 μm. **c** Quantification of the distribution of GFP-positive neurons, At least three brains from each genotype were analyzed. Student's *t* test was performed to compare two groups, n.s. not significant. Error bars show mean ± SEM. **d** Quantification of the number of multipolar and bipolar/monopolar neurons. At least three brains from each genotype were analyzed. Student's *t* test was performed to compare two groups, n.s. not significant. Error bars show mean ± SEM. **e** Schematic of time-lapse imaging after IUE. **f** Representative images of migrating neurons in organotypic cortical slice cultures from WT brains. **g** Representative images of migrating neurons in organotypic cortical slice cultures from Tcf4 cKO brains. **h**, **i** Representative neuronal migration tracks in WT (**h**) and Tcf4 cKO (**i**) brains. **j** Quantification of neuronal migration speed in the IZ and CP respectively, Student's *t* test was performed to compare two groups, $^{**}p < 0.01$. Error bars show mean ± s.e.m.

Tcf4 is required for the postnatal positioning of neurons in the cortex

Given the normal migration of Tcf4-deficient neurons during embryonic stages, we reasoned that Tcf4 may be required for neuronal positioning when postnatal migration is complete. We utilized the birthdate-dependent "inside-out" neuronal layering pattern and performed sequential *in utero* electroporation to evaluate the positions of neurons produced at different developmental stages (Fig. 3). We first electroporated plasmids expressing Cre recombinase fused with GFP into cortical progenitor cells of $Tcf4^{f/f}$ or WT brains *in utero* at E14.5. Consequently, Cre recombinase-mediated recombination

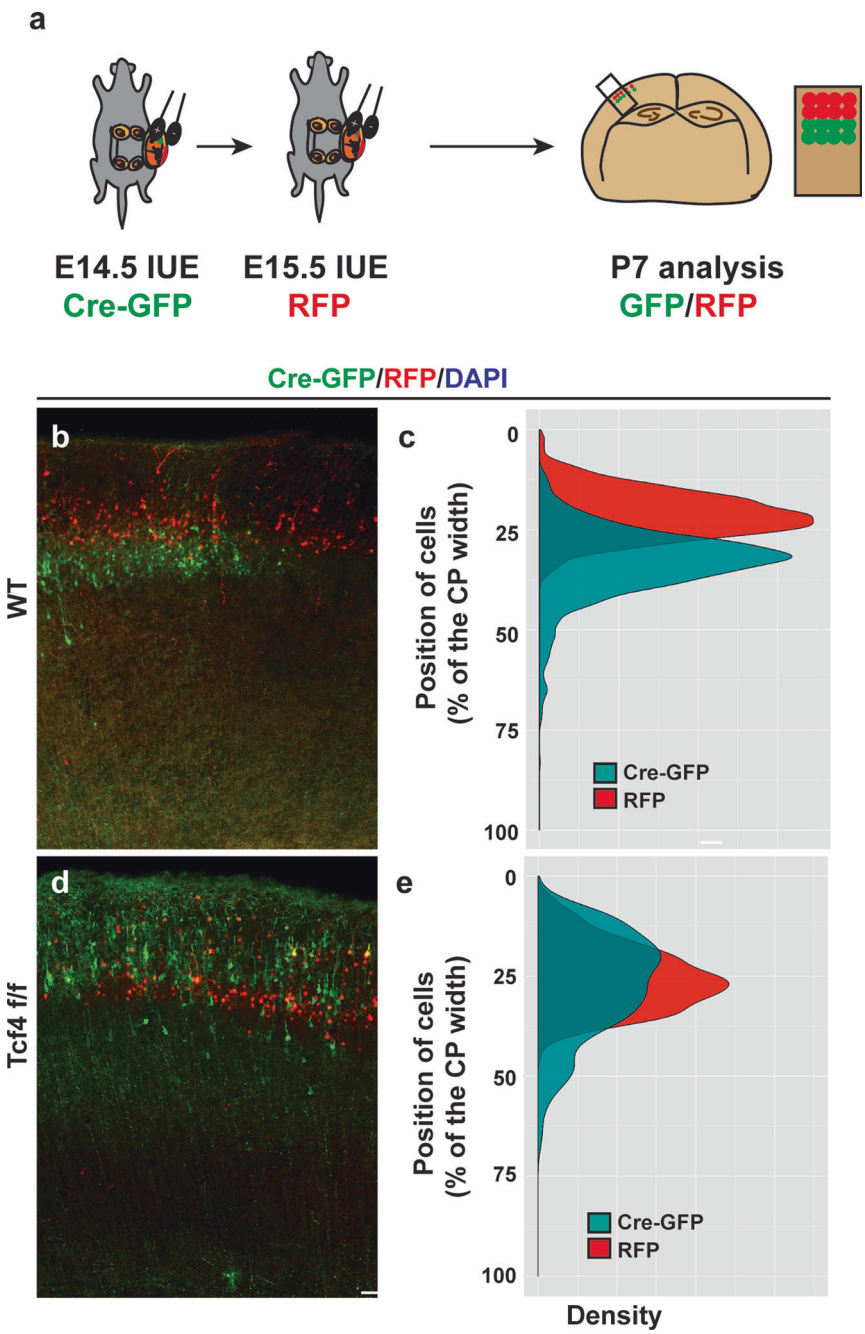

Fig. 3 Abnormal positioning of Tcf4-deficient neurons. **a** Schematic of sequential IUE. **b** Representative image for the sequential IUE in WT brains. **c** Quantification of neuronal positioning in WT brains, At least three brains were analyzed. **d** Representative image for the sequential IUE in Tcf4$^{f/f}$ brains. **e** Quantification of neuronal positioning in Tcf4$^{f/f}$ brains. At least three brains were analyzed.

would generate neurons lacking Tcf4 that are labeled by GFP in Tcf4$^{f/f}$ brains. To label neurons born later, we introduced a vector expressing red fluorescent protein (RFP) 24 h after the first electroporation in both WT and Tcf4$^{f/f}$ brains (Fig. 3a). At P7, early-born neurons labeled with GFP and late-born neurons labeled with RFP were clearly segregated into two layers in a birthdate-dependent manner in WT brains (Fig. 3b, c). In contrast, early-born Tcf4-deficient neurons (GFP-positive) did not localize normally to form a cohesive layer and were positioned close to the basal membrane, although the late-born neurons (RFP-positive) were localized normally (Fig. 3d, e). We observed that most RFP-positive neurons were not positive for GFP in Tcf4$^{f/f}$ brains (95.8 ± 1.16% in Tcf4 cKO brains compared to 92.44 ± 1.31% in WT brains), suggesting that most of these neurons were WT neurons. We noticed that RFP-positive cells in Tcf4$^{f/f}$ brains seemed to be located deeper than in WT brains (Fig. 3c, e), likely due to a non-cell-autonomous effect. Taken together, these data suggest that Tcf4 loss leads to neuronal mispositioning in the postnatal stage.

Abnormal orientation of Tcf4-deficient neurons

The formation of postnatal clusters in Tcf4 cKO brains likely results from abnormal neuronal movement. Therefore, we next characterized the orientation of Tcf4-deficient neurons in the clusters. For this, we electroporated plasmids expressing either GFP or Cre-GFP into the neural progenitor cells of $Tcf4^{f/f}$ brains at E15.5 and analyzed them at P7 (Supplementary Fig. S8). In WT brains, the neurons were evenly distributed in the upper layer cortex and oriented parallel to the apical-basal axis (Supplementary Fig. S8a). However, Tcf4-deficient neurons were located close to the pia and formed clusters (Supplementary Fig. S8b). When we examined the orientation of these neurons, we found that Tcf4-deficient neurons were randomly positioned compared with neurons in WT brains. Quantification of the angle between the apical-basal axis of neurons and the pia showed that most of the Tcf4-deficient neurons in the clusters were randomly oriented (Supplementary Fig. S8c), likely impairing their subsequent positioning. In addition, we also observed that the dendritic arbors of Tcf4-deficient neurons became abnormal (Supplementary Fig. S8d, e). Taken together, these findings show that neurons lacking Tcf4 could not position themselves properly after migration to the CP and displayed abnormal orientation in the clusters.

Deficiency of Tcf4 leads to neuronal clustering with enhanced movement

To examine the dynamic formation of neuronal clusters in Tcf4-deficient brains, we performed time-lapse imaging of brain slices to monitor neuronal movement directly in the postnatal stages. Electroporation of a vector expressing GFP into either WT or Tcf4 cKO cortices was performed at E14.5 and sections were imaged at P2 for ~24 h (Fig. 4a). In control brains, neurons did not undergo dramatic movements, and most of the cells remained at the same position over time (Fig. 4b). In contrast, we observed that neurons of Tcf4 cKO brains moved closer to each other and ultimately formed clusters (Fig. 4c). To further analyze the spatial distribution of these GFP-positive neurons quantitatively, we performed nearest-neighbor distance (NND) analysis and found that the NNDs among the Tcf4-deficient neurons were significantly shorter than those of WT neurons (Fig. 4d). Analysis of neuronal movement showed that Tcf4-deficient neurons moved over a long distance in various directions, while most WT neurons moved within a short distance along the apical-basal axis (Fig. 4e–i). In addition to abnormal movement, Tcf4-deficient neurons also showed dynamic changes in their processes (Supplementary Fig. S9), which could prevent them from anchoring at the basal membrane. Therefore, these data demonstrate that Tcf4-depleted neurons retain enhanced movement activity and cluster together within the postnatal cortex.

Cell adhesion molecule expression is dysregulated in Tcf4 cKO brains

To further investigate the mechanisms by which Tcf4 regulates neuronal positioning during brain development, we performed global transcriptome analysis of cortical tissue collected from both WT and Tcf4 cKO brains at P0 shortly before obvious neuronal mispositioning occurred. RNA sequencing (RNA-seq) revealed both up- and downregulated genes (1515 genes and 1439 genes, respectively) in Tcf4 cKO brains compared to WT brains (FDR < 0.05) (Fig. 5a). We then subjected the differentially expressed genes to gene ontology (GO) analysis, which revealed enrichment for genes involved in brain development (Fig. 5b). Intriguingly, the category with the highest p-value was cell adhesion (Fig. 5b). Cell adhesion has been demonstrated to play essential roles in the regulation of neuronal movement [14, 32, 33]. Thus, these data suggest that Tcf4 controls neuronal positioning through the transcriptional regulation of cell adhesion molecules.

Tcf4 controls neuronal positioning through Fn1

Among the downregulated genes related to cell adhesion in Tcf4 cKO cortices compared to WT cortices, one of the most significantly dysregulated genes is Fn1, a cell adhesion molecule highly expressed in the upper layer neurons [34]. In situ hybridization was performed to further confirm the downregulation of Fn1 expression upon the loss of Tcf4 (Fig. 5c, d). We then asked whether Fn1 downregulation could cause neuronal mispositioning, as we observed in Tcf4 cKO brains. Indeed, when Fn1 was downregulated by shRNA interference, we found that neurons were mispositioned compared to those of control brains, which could be rescued by restoring the expression of Fn1 (Fig. 5e–h). Intriguingly, we found that some neurons formed clusters close to the basal membrane when Fn1 was downregulated (Fig. 5f, arrowheads). Downregulation of Fn1 did not result in obvious defects in neural progenitor proliferation and differentiation (Supplementary Fig. S10). To further demonstrate that Fn1 is a key downstream effector of Tcf4, we examined whether the forced expression of Fn1 in Tcf4-deficient neurons could attenuate mispositioning. We then electroporated constructs expressing Cre recombinase alone or together with constructs expressing Fn1 into RGPs *in utero* at E14.5. The electroporated brains were analyzed at P7 (Fig. 5i–l). Compared to control brains, Tcf4 cKO brains showed neuronal mispositioning (Fig. 5j). In addition, the expression of Fn1 in Tcf4-deficient neurons resulted in a marked attenuation of the positioning defect

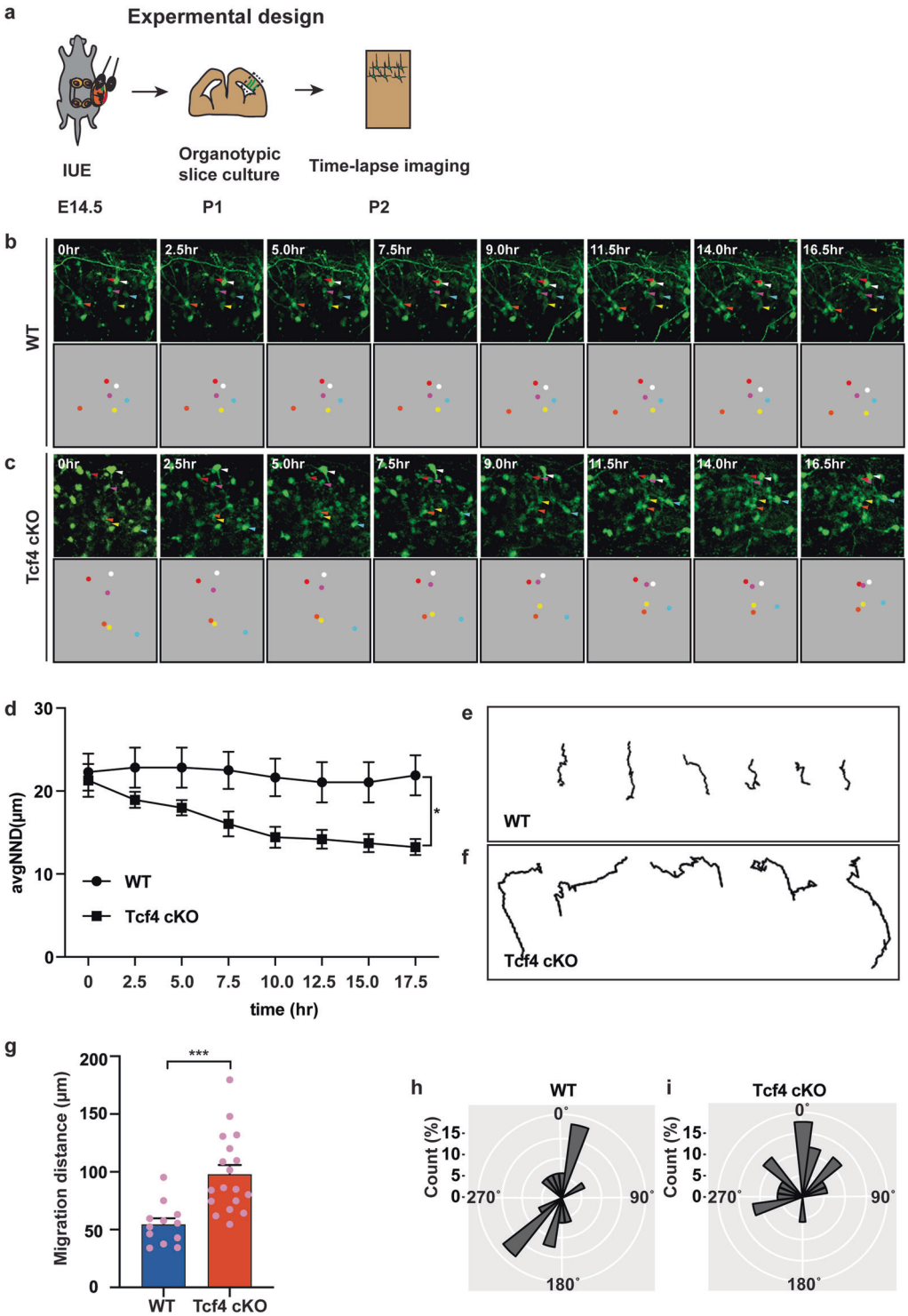

Fig. 4 Neurons become clustered upon the loss of Tcf4. a Experimental design for time-lapse imaging. **b** Representative images for the movement of neurons in WT brains. **c** Representative images for the movement of neurons in Tcf4 cKO brains. **d** Nearest-neighbor distance (NND) analysis of neurons imaged in WT and Tcf4 cKO brains, two-way ANOVA, $*P < 0.05$. **e**, **f** Neuronal migration tracks from WT (**e**) and Tcf4 cKO (**f**) brains. **g** Quantification of the neuronal migration distance within a time unit, Student *t* test was performed, $***p < 0.001$. At least three brains were analyzed for each genotype. **h, i** Distribution of angles between the line perpendicular to the pia and the line connected the starting and the ending points of a neuronal movement track.

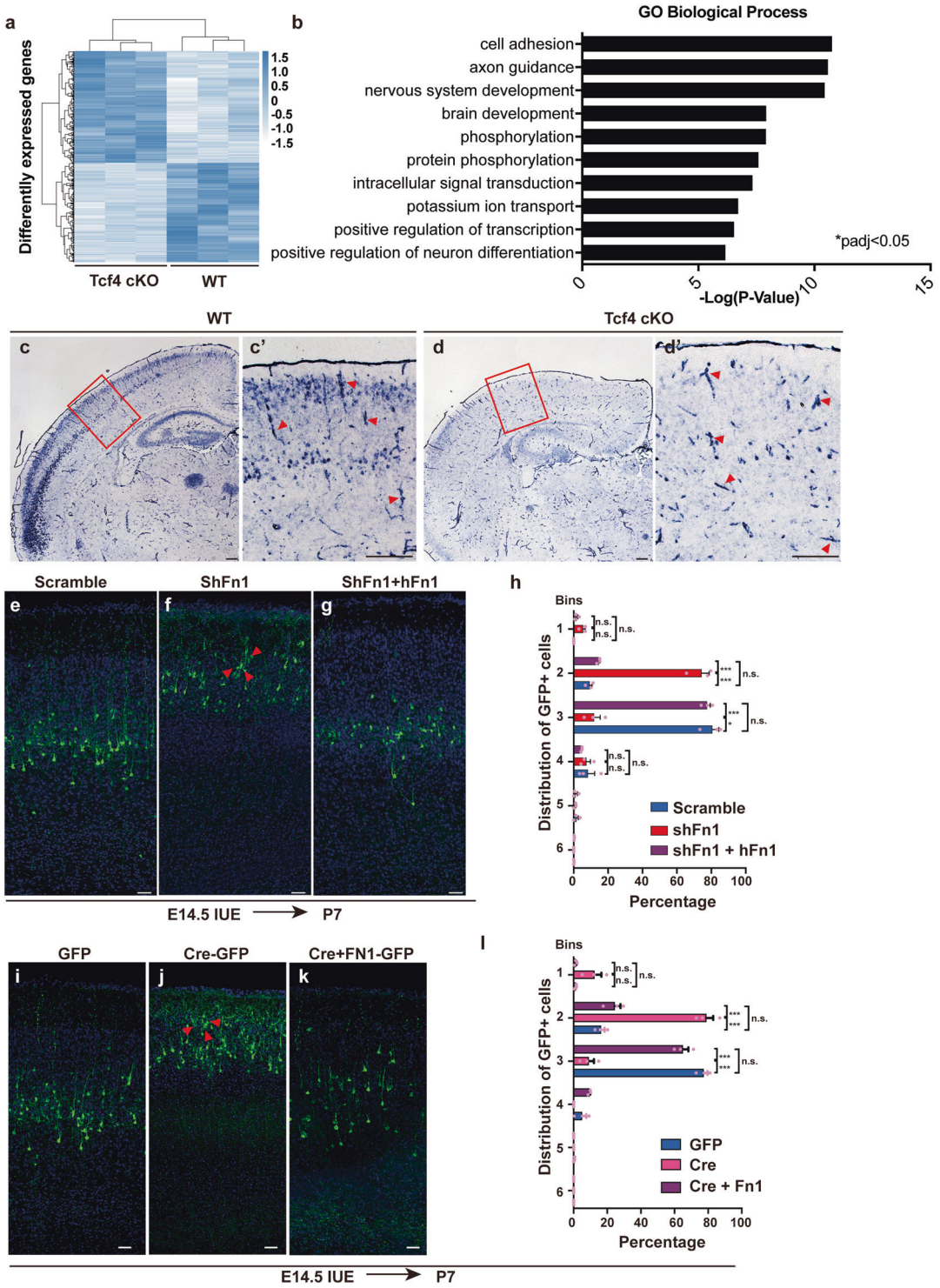

and migration speed (Fig. 5k, i, Supplementary Fig. S11). The morphological defects in Tcf4-deficient neurons were also largely rescued by the forced expression of Fn1 (Supplementary Fig. S12). Taken together, these data suggest that Fn1 is an important downstream effector of Tcf4 in the regulations of neuronal positioning.

Abnormal neuronal functions in Tcf4-deficient brains

Neuronal mispositioning within the cortex could have potential effects on the neuronal network. Pyramidal neurons born at E14.5 and E16.5 migrate to cortical layers 4

◀ **Fig. 5 Tcf4 acts through Fn1 to regulate neuronal positioning.** **a** Heatmap of the genes expressed differentially between Tcf4 cKO and WT cortices. 1515 genes are upregulated and 1439 genes are downregulated. padj < 0.05. **b** Gene ontology (GO) analysis of the differentially expressed genes. **c**, **d** Expression of Fn1 was examined by in situ hybridization in WT (**c**) and Tcf4 **c**KO (**d**) brains at P7. Enlarged images are shown in **c′** and **d′**. Arrowheads in **c′** and **d′** indicate the blood vessels. Scale bar: 200 µm. **e–g** Downregulation of Fn1 (**f**) leads to neuronal mispositioning compared to scramble electroporated brains (**e**), which is rescued by the expression of Fn1 (**g**) Arrowheads show a neuronal cluster. Scale bar: 50 µm. **h** Quantification of the distribution of GFP-positive neurons and the cortex is evenly divided as six bins. One-way ANOVA and Turkey's multiple comparisons test was performed. Error bars show mean ± SEM. $^{**}p < 0.01$, $^{***}p < 0.001$. **i–k** Overexpression of Fn1 attenuates the abnormal positioning caused by the loss of Tcf4 (**k**) compared to Cre electroporated brains (**j**). Constructs expressing GFP were electroporated as control (**i**). Scale bar: 50 µm. **l** Quantification of the distribution of GFP-positive neurons and the cortex is evenly divided as six bins. One-way ANOVA and Turkey's multiple comparisons test was performed. Error bars show mean ± SEM.$^{**}p < 0.01$, $^{***}p < 0.001$, n.s. not significant.

and 2/3, respectively. In the canonical cortical circuit, pyramidal neurons in layer 4 send excitatory inputs to neurons in layers 2/3, but not vice versa (Fig. 6a) [35]. We reasoned that Tcf4-deficient neurons mispositioned in layers 2/3 might cause a change in cortical microcircuits. To test this hypothesis, we electroporated plasmids expressing GFP or CAG-Cre-GFP into cortical progenitor cells *in utero* at E14.5 to label early-born layer 4 neurons. At E16.5, we then electroporated the same embryos with plasmids expressing ChR2-mCherry to label late-born layer 2/3 neurons. Short blue light stimulation (5 ms) evoked action potentials in mCherry-positive neurons (Fig. 6a). In GFP-electroporated brains, all GFP-positive neurons did not respond to the light stimulation. However, we observed that excitatory postsynaptic potentials (EPSPs) were evoked in many Tcf4-deficient neurons (CAG-Cre-GFP-positive neurons) in layers 2/3 by light stimulation (Fig. 6b, c). Interestingly, the ratio of Tcf4-deficient neurons responding to light stimulation decreased when mispositioning was rescued by the expression of Fn1 (Fig. 6b, c). Taken together, these results suggest that cortical microcircuits are disrupted when Tcf4-deficient neurons are mispositioned.

To further test the effects of neuronal mispositioning on the function of Tcf4-deficient neurons, we used the primary visual cortex (V1) as a model system, as it is a well-organized brain region where specific neuronal projections and locations undergo precise arrangement and refinement during development [36, 37]. Thus, visual functions such as orientation tuning, retinotopy, and ocular dominance columns are established based on the precise location and connections between specific neurons [38, 39]. To examine whether neuronal functions were disrupted in Tcf4-deficient mice, we first examined V1 by measuring the expression of c-fos, an immediate-early gene, triggered by light exposure (Fig. 6d) [40]. While the expression level of c-fos remained similarly low in the visual cortex of both WT and Tcf4 cKO brains when the mice were kept in the dark (Fig. 6e, f), we detected significantly lower expression of c-fos in the visual cortex of Tcf4 cKO mice than in that of WT mice after exposure to normal light for 1 h after 72 h of complete darkness (Fig. 6g–i). To further confirm the deficiency of visual responses in Tcf4 cKO mice, we performed in vivo extracellular electrophysiology in the V1 neurons of both WT and Tcf4 cKO mice. The drifting grating visual stimulus-evoked robust spiking of the V1 neurons in WT mice (Fig. 6j). However, we found that visually evoked spiking of V1 neurons in Tcf4 cKO mice was significantly reduced, while spontaneous activity was not affected, which resulted in a significant reduction in the signal-to-noise ratio in Tcf4 cKO mice (Fig. 6k, l). When examining the visually evoked potentials (VEPs), which represent the synchronized visual responses of a large number of neurons, we observed that Tcf4 cKO mice showed a significant reduction in VEP amplitudes in V1 compared to those of WT controls, indicating that knocking out Tcf4 disrupted the synchronized visual responses in mouse V1 neurons (Fig. 6m). Therefore, these data suggest that neuronal mispositioning caused by Tcf4-deficiency disrupts neuronal functions.

Discussion

Precise positioning of cortical neurons is essential for proper functioning. Here, we revealed an essential role for Tcf4 in regulating neuronal positioning during cortical development. Depletion of Tcf4 leads to neuronal mispositioning, while the migration of neurons towards the CP is largely unaffected. Neuronal mispositioning in Tcf4-deficient brains is achieved through the downregulation of cell adhesion molecules. In particular, we identified Fn1 as a key downstream effector of Tcf4 in the regulation of neuronal positioning. Furthermore, we found that depletion of Tcf4 leads to the disruption of neuronal function. Our findings reveal the importance of neuronal positioning in brain development. Interestingly, the phenotype of neuronal clusters in the Tcf4 cKO neocortex is reminiscent of the entorhinal cortex [41, 42]. When examining the expression of Tcf4 in the embryonic entorhinal cortex (the Allen Developmental Mouse Brain Atlas), we found the expression of Tcf4 is low in these areas compared to the other brain regions. It is possible that the formation of clusters in these areas is correlated with the Tcf4 expression. However, the entorhinal cortex has a different developmental process and the existence of cell clusters in the entorhinal cortex could occur with other mechanisms.

Disruption of birthdate-dependent neuronal positioning in the neocortex has been linked to many brain disorders

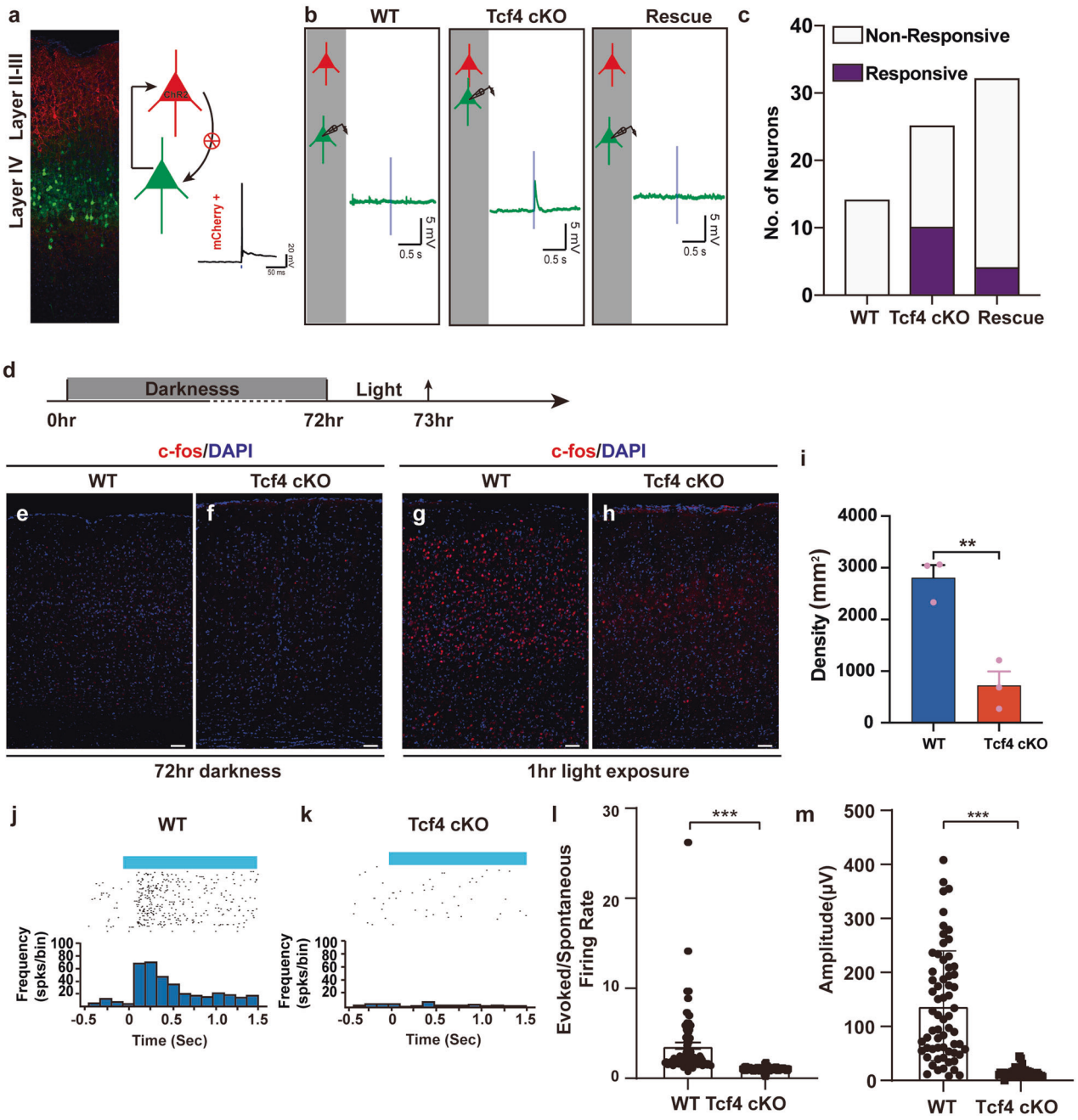

Fig. 6 Disruption of the neuronal function upon the loss of Tcf4. **a** Left: the representative image showing neurons expressing ChR2-mCherry and GFP in layers 2/3 and layer 4 cortex in the normal condition. Right: schematic showing neuronal connections between layers 2/3 and layer 4. **b** Response traces of neurons labeled with GFP when activating ChR2-mCherry-positive neurons by blue light stimulation in WT, Tcf4 cKO, and Rescue slices. **c** Quantification of responsive neurons. 14 neurons from 2 WT mice, 25 neurons from 4 Tcf4 cKO mice, and 32 neurons from 5 mice in rescue group were used. **d** Experimental design for visual response. **e**–**h** Representative images of sections stained for c-fos. **i** Quantification of the density of c-fos-positive cells. At least three brains were analyzed in each genotype. Student *t* test was performed, error bars show mean ± SEM. $^{**}p < 0.01$. **j**, **k** Examples of raster plots and peristimulus time histogram showing spiking activities during sinusoidal drifting gratings stimulation in WT (**j**) and Tcf4 cKO (**k**) mice, respectively. Blue bar represented visual stimulation. **l** The average ratio of evoked to spontaneous activities in the V1 of WT and Tcf4 cKO mice during visual stimulation. 117 units from 4 WT mice and 150 units from 3 Tcf4 cKO mice were analyzed, Student's *t* test was performed, $^{**}p < 0.01$. **m** Average VEP amplitudes to visual stimuli presented to the WT and Tcf4 cKO mice. 64 VEPs from 4 WT mice and 49 VEPs from 3 Tcf4 cKO mice were analyzed, Student's *t* test was performed, $^{**}p < 0.01$.

[43–47], indicating the importance of proper neuronal positioning. However, little is known regarding how neurons maintain their positions within the cortex after migration, as prior analyses of neuronal mispositioning have largely focused on the consequence of defects in the migration of neurons to their destinations. Here, we found that the depletion of Tcf4 leads to neuronal clustering when neuron migration concludes in the early postnatal stages, while the migration of neurons towards the CP in embryonic stages is largely unaffected, suggesting that Tcf4 is required for neuronal rearrangement after migration. These findings reveal the importance of Tcf4 in early developmental stages of the brain, which could contribute to neuronal functions in the adult brain.

Interestingly, the expression of *Fn1* is high in the CP during the early postnatal stages and is nearly undetectable in cortical neurons during the embryonic stages (the Allen Developmental Mouse Brain Atlas, data not shown), potentially explaining why Tcf4 regulates neuronal positioning acting via Fn1 in the early postanal stages. Fibronectin plays essential roles in cell adhesion through interactions with the extracellular matrix [48]. Thus, the abolishment of Fn1 expression in Tcf4 mutant cells could reduce the adhesion of neurons to the extracellular matrix or neighboring cells. During mesenchymal-ameboid transition, slow mesenchymal cells can switch to fast ameboid migration under the condition of low adhesion [33], suggesting that a well-controlled level of adhesion is important for cell movement. The increase in the migration speed of cells under low adhesion could lead to clustering. Indeed, when cells are plated on nonadhesive substrates, they become aggregated over time [49]. In migrating neurons, disruption of adhesion molecules leads to an imbalance in the attraction and repulsion between cells and leads to an increase in migration speed [14]. Therefore, it is likely that the reduction of Fn1 mediated by the loss of Tcf4 leads to the reduction of cell adhesion and thereby causes increased cell movement (Fig. 4), ultimately leading to the formation of neuronal clusters. When analyzing the dysregulated genes in the RNAseq results, particularly, cell adhesion molecules, we found that several genes involved in the repulsive guidance of neuronal migration were downregulated. For example, Flrt3, a fibronectin leucine-rich transmembrane protein, functions as a heterophilic chemorepellent [14] and is downregulated in Tcf4 cKO brains. Therefore, it is likely that the balance between attraction and repulsion is affected in Tcf4 cKO brains. However, the details of the underlying mechanisms require further investigation in the future. Thus, the transcriptional regulation of cell adhesion molecules is essential for neuronal positioning in the cortex.

Taken together, these results reveal a crucial role for Tcf4 in controlling neuronal positioning after migration is finalized during brain development and highlight the importance of proper neuronal positioning for the establishment of functional neuronal circuits. Positional strategies are important for specific neuronal connections [50], and neuronal mispositioning could lead to the disruption of neuronal function. Intriguingly, patches of neuronal disorganization in the neocortex have been found in patients with autism [51]. Therefore, our results not only provide novel insights into the basis of neurological defects linked to TCF4 mutations but also provide a potential link between neuronal disorganization and psychiatric disorders.

Material and methods

Experimental animals

Homozygous $Tcf4^{f/f}$ mice in which the fragments containing the bHLH exons and the 3′ exons are flanked by loxP sites were crossed with Emx1-Cre mice [24, 25] to generate $Tcf4^{f/+}$; Emx1Cre mice, which were further crossed with $Tcf4^{f/f}$ mice to generate $Tcf4^{f/f}$; Emx1Cre mice (Tcf4 cKO). All animal work was approved by Animal Care and Use Committee of Shanghai Medical College of Fudan University.

Immunohistochemistry

Embryonic brains were harvested and then fixed in 4% Paraformaldehyde (PFA) overnight except the brains stained for Tbr2, which was fixed for 5 h. Then fixed brains were dehydrated in 30% sucrose dissolved in PBS solution until the sample sunk to the bottom at 4 °C. For postnatal brain samples, pups were anesthetized on ice, and cardiac perfusion was performed with 4% PFA before overnight fixation with 4% PFA followed by dehydration in 30% sucrose. Frozen sections were prepared for immunostaining and were first permeabilized in 0.5% Triton-X in PBS for 30 min followed by the incubation of desired primary antibody at 4 °C for overnight. After washing, the secondary antibody was incubated in darkness for 2 h at room temperature. DAPI staining was performed before mounting.

Sequential *in utero* electroporation

Timed pregnant mice were anesthetized and embryos were electroporated according to an established protocol published before [52]. Embryos were electroporated with plasmids expressing Cre and GFP both driven by the CAG promoter to generated mutant neurons in $Tcf4^{f/f}$ background. 24 h later at E15.5, electroporated embryos were given a second electroporation with constructs expressing RFP driven by the CAG promoter to label WT neurons. Electroporated brains were harvested to analyze at P7.

Time-lapse imaging

Time-lapse imaging was performed according to a protocol published recently [52]. Electroporated brains were embedded in 4% low-melting agarose (Fisher Scientific, BP165-25) in artificial cerebrospinal fluid (ACSF, 125 mM NaCl, 2 mM $CaCl_2$, 2.5 mM KCl, 1 mM MgCl, 1.25 mM NaH_2PO_4, 25 mM $NaHCO_3$, and 25 mM Glucose) and sectioned into 300 μm slices using a vibratome (LEICA VT1200S). After transferred onto a cell culture insert (Millicell PIMORG50) in a glass-bottom dish (Thermo Scientific, 150682), brain slices were cultured in the culture medium (25% HBSS, 66% BEM, 5% FBS, 1% penicillin/streptomycin, N_2 supplements (all from Thermo Scientific), and 6% Glucose (Sigma)). After overnight culture, brain slices containing GFP-expressing cells were imaged using an inverted confocal microscope (Nikon ECLIPSE Ti) for about 24 h.

In situ hybridization

In situ hybridization was performed according to a recent published protocol [53]. The following primers were used to generate *Fn1* probes:

Fwd: 5′- GACGCACCATCCAACCTGCGG

Rew: 5′- CCTCCTCATCTACATTCGGCA

In vitro electrophysiology

Mouse brain slices were prepared according to the published procedures [54]. Mice were anesthetized by isoflurane, and brains were rapidly removed and immersed into ice-cold, oxygenated (95% O_2/5% CO_2) artificial cerebrospinal fluid (ACSF) containing 140 mM NaCl, 5 mM KCl, 15 mM Glucose, 10 mM HEPES and 2 mM $CaCl_2$. Tissues were blocked and supported by a small block of 4% agar, and transferred to a slicing chamber containing ice-cold ACSF. Coronal slices of 250 μm thickness were cut on a vibratome (Series1000, Tissue Sectioning System, Natural Genetic Ltd., USA) in a rostral/caudal direction and transferred into a holding chamber with ACSF, equilibrated with 95% O_2/5% CO_2. Slices were incubated at 34 °C for ~30 min before recording. Brain slices were transferred to a recording chamber perfused with oxygenated ACSF at room temperature. Neurons expressing GFP in the cortex were located and recorded using patch pipettes of ~4–7 MΩ resistance. The solution in recording pipettes consisted of (in mM): 135 K-gluconate, 4 KCl, 5 $MgCl_2$, 20 HEPES, 2 MgATP, 0.2 Na_2GTP, and 1 EGTA (pH 7.2, ~295 mOsm/L). Whole-cell recordings were made using an 700B amplifier and Digidata 1440 A interface (Axon Instruments, Union City, CA). Signals were filtered at 4 kHz, sampled at 10 kHz, and analyzed using Clampex 10.7. To activate ChR2-expressing fibers of pyramidal neurons in the cortex, light stimulation (470 nm, ~5–10 mW) was delivered at the recording site through a ×40 water-immersion objective (Olympus, Tokyo, Japan) using the Polygon 400 system (Mightex, USA).

In vivo recording

Mice were sedated with chlorprothixene (1.25 mg/kg in DMSO, i.m.) and then anesthetized with urethane (1.25 g/kg in 10% saline solution, i.p.). Atropine (0.3 mg/kg, in 10 % saline) and dexamethasone (2 mg/kg, in 10% saline) were administrated subcutaneously, as described before [55]. The skin covering the scalp was removed to expose the skull. A metalhead plate was implanted on top of the skull with Super-Bond (C&B, Japan), and the plate was then mounted to a stand on the vibration isolation table. A thin layer of silicone oil was applied to both eyes to prevent drying. A small craniotomy (~1.5 mm^2) was made on the skull to expose binocular V1. The center of the craniotomy was 3.0 mm lateral and 0.5 mm anterior from the Lambda point. The exposed brain was kept moist with ACSF. Throughout recordings, toe-pinch reflex was monitored and additional urethane (0.2–0.3 g/kg) was supplemented as needed. The animals' temperature was monitored with a rectal thermoprobe and maintained at 37 °C through a feedback heater (Harvard Apparatus, USA).

For in vivo recording, Tungsten electrodes (5–10 MΩ, FHC, Bowdoinham, ME) were inserted perpendicular to the pial surface. Recording sites were 200–600 μm below the pial surface, spanning all the layers of the visual cortex. Electrical signals were filtered between 0.3 and 8.0 kHz for single-unit spiking, and between 0.05 and 200 Hz for VEPs and sampled at 40 kHz using an OmniPlex-D System (Plexon, Dallas, USA). The spike waveforms were sorted offline with Offline Sorter (v3.0) (Plexon Inc, USA) to isolate single units as described before [55].

Stimuli were presented using a LCD monitor (40 × 30 cm, 60 Hz refresh rate, 100% contrast, ~30 cd/m^2 luminance) placed 20 cm in front of the animal. For orientation selectivity, sinusoidal gratings drifting perpendicular to their orientations were generated with the PsychoPy (v3.00) package. The direction of the gratings varied between 0° and 330° (12 steps at 30° spacing) in a pseudorandom sequence. Spatial frequency of the stimuli was set at 0.04 cycle/degree. Temporal frequency was set at 2 Hz. Each stimulus was presented for 1.5 s (three cycles), with 1.5 s inter-stimulus interval. For spatial frequency preference, square gratings reversing at 1 Hz were used. Spatial frequency of the gratings was pseudo-randomized among 0.04, 0.08, 0.16, 0.32, 0.64 cycle/degree, as described before [56].

To calculate the visually-evoked spiking response (R), spontaneous spiking rate was subtracted from the total rate at each stimulus condition. To determine the preferred

orientation and degree of selectivity, we calculated $\frac{\sum R(\theta)e^{2i\theta}}{\sum R(\theta)}$, where $R(\theta)$ is the evoked spiking responses at θ direction of gratings. Its amplitude was used as a global orientation-selective index. Half of its complex phase was calculated [57] and then converted to the preferred orientation (pref_O) by subtracting 90°, to confine pref_O between −90° to 90°.

RNAseq and analysis

Total RNA was isolated from both WT and Tcf4 cKO cerebral cortices at P0 using TRIzol reagent (ThermoScientific). RNAseq was performed at Genomics Core Facility of Shanghai Center for Plant Stress Biology, CAS. Sequencing raw reads were applied quality and adapter trimming using trim_galore with a quality cutoff of 30. Cleaned reads were mapped to the mouse reference genome UCSC mm10. Differential expression analysis was performed using DESeq2 with a cutoff of FDR < 0.05. RNA sequencing data was deposited as GEO accession: GSE166412.

DiI labeling

To label the radial glia processes, embryonic brains from both WT and Tcf4 cKO mice were fixed with 1% PFA at 4 °C for 4 h and then DiI (1ug/ul dissolved in DMSO, ThermoScientific) was injected into the ventricular using a glass pipet. After incubation at 37 °C in 4% PFA for 2 days, brains were embedded with 2% agarose and cut into 70 μm slices using a vibratome.

Image acquiring and analysis

Images were acquired using Nikon A1R microscopy. Images were processed using NIS-Elements AR (Nikon) or Adobe Photoshop CC. For data analysis, Prism 6 or Excel was used. Data collection and analysis were performed without blindness to the conditions of the experiments due to the obvious phenotype in mutants. Data are presented as mean ± SEM. $P < 0.05$ was considered significant. Significance is marked as $*p < 0.05$; $**p < 0.01$ and $***p < 0.001$. At least three brains were used for each phenotype analyzed.

Acknowledgements We thank all members of the Xie lab for discussions. We thank Drs. T. Behnish and Y. Jiang for critical reading the manuscript. We thank the IOBS Core facility for expert microscopy. This study was supported by the National Key Research and Development Program of China (grant no. 2018YFA0108000), the National Natural Science Foundation of China (grant nos. 31872763, 31471038, 81828008), Shanghai Municipal Science and Technology Major Project (No.2018SHZDZX01, 19JC1411003) and ZJLab to YX and the National Natural Science Foundation of China (grant nos. 31872764, 81800862), Shanghai Science and Technology Committee (grant no. 19QA1401600) to YG, Shanghai Pujiang Program (19PJ1401800) to LX.

Author contributions YX conceived and designed the project. Yandong Z performed experiments and analyzed the data with help from CZ, WY, LZ, Yilan Z, and TT, GH, NL, QL, and YG performed and analyzed in vivo recording experiments. SH, SC, and LX performed and analyzed in vitro recording experiments. YX performed experiments, analyzed the data, and wrote the manuscript with comments from other authors.

Compliance with ethical standards

Conflict of interest The authors declare no competing interests.

Publisher's note Springer Nature remains neutral with regard to jurisdictional claims in published maps and institutional affiliations.

References

1. Kriegstein A, Noctor S, Martinez-Cerdeno V. Patterns of neural stem and progenitor cell division may underlie evolutionary cortical expansion. Nat Rev Neurosci. 2006;7:883–90.
2. Ambrozkiewicz MC, Schwark M, Kishimoto-Suga M, Borisova E, Hori K, Salazar-Lázaro A, et al. Polarity acquisition in cortical neurons is driven by synergistic action of Sox9-regulated Wwp1 and Wwp2 E3 ubiquitin ligases and intronic miR-140. Neuron. 2018;100:1097–.e15.
3. Cooper JA. Molecules and mechanisms that regulate multipolar migration in the intermediate zone. Front Cell Neurosci. 2014;8:386.
4. Nadarajah B, Brunstrom JE, Grutzendler J, Wong RO, Pearlman AL. Two modes of radial migration in early development of the cerebral cortex. Nat Neurosci. 2001;4:143–50.
5. Kriegstein A, Alvarez-Buylla A. The glial nature of embryonic and adult neural stem cells. Annu Rev Neurosci. 2009;32:149–84.
6. Taverna E, Götz M, Huttner WB. The cell biology of neurogenesis: toward an understanding of the development and evolution of the neocortex. Annu Rev Cell Dev Biol. 2014;30:465–502.
7. Rakic P. Evolution of the neocortex: a perspective from developmental biology. Nat Rev Neurosci. 2009;10:724–35.
8. Romero DM, Bahi-Buisson N, Francis F. Genetics and mechanisms leading to human cortical malformations. Semin Cell Dev Biol. 2018;76:33–75.
9. Valiente M, Marin O. Neuronal migration mechanisms in development and disease. Curr Opin Neurobiol. 2010;20:68–78.
10. Kawauchi T. Cellullar insights into cerebral cortical development: focusing on the locomotion mode of neuronal migration. Front Cell Neurosci. 2015;9:394.
11. Cooper JA. Cell biology in neuroscience: mechanisms of cell migration in the nervous system. J Cell Biol. 2013;202:725–34.
12. Sekine K, Kawauchi T, Kubo K, Honda T, Herz J, Hattori M, et al. Reelin controls neuronal positioning by promoting cell-matrix adhesion via inside-out activation of integrin α5β1. Neuron. 2012;76:353–69.
13. Kawauchi T, Sekine K, Shikanai M, Chihama K, Tomita K, Kubo K, et al. Rab GTPases-dependent endocytic pathways regulate neuronal migration and maturation through N-cadherin trafficking. Neuron. 2010;67:588–602.
14. Del Toro D, Ruff T, Cederfjäll E, Villalba A, Seyit-Bremer G, Borrell V, et al. Regulation of cerebral cortex folding by controlling neuronal migration via FLRT adhesion molecules. Cell. 2017;169:621–.e16.

15. Franco SJ, Martinez-Garay I, Gil-Sanz C, Harkins-Perry SR, Muller U. Reelin regulates cadherin function via Dab1/Rap1 to control neuronal migration and lamination in the neocortex. Neuron. 2011;69:482–97.
16. Jossin Y, Cooper JA. Reelin, Rap1 and N-cadherin orient the migration of multipolar neurons in the developing neocortex. Nat Neurosci. 2011;14:697–703.
17. Jung M, Häberle BM, Tschaikowsky T, Wittmann MT, Balta EA, Stadler VC, et al. Analysis of the expression pattern of the schizophrenia-risk and intellectual disability gene TCF4 in the developing and adult brain suggests a role in development and plasticity of cortical and hippocampal neurons. Mol Autism. 2018;9:20.
18. de Pontual L, Mathieu Y, Golzio C, Rio M, Malan V, Boddaert N, et al. Mutational, functional, and expression studies of the TCF4 gene in Pitt–Hopkins syndrome. Hum Mutat. 2009;30:669–76.
19. Sweatt JD. Pitt–Hopkins Syndrome: intellectual disability due to loss of TCF4-regulated gene transcription. Exp Mol Med. 2013;45:e21.
20. Forrest MP, Hill MJ, Quantock AJ, Martin-Rendon E, Blake DJ. The emerging roles of TCF4 in disease and development. Trends Mol Med. 2014;20:322–31.
21. Forrest MP, Hill MJ, Kavanagh DH, Tansey KE, Waite AJ, Blake DJ. The Psychiatric Risk Gene Transcription Factor 4 (TCF4) regulates neurodevelopmental pathways associated with schizophrenia, autism, and intellectual disability. Schizophr Bull. 2018;44:1100–10.
22. Blake DJ, Forrest M, Chapman RM, Tinsley CL, O'Donovan MC, Owen MJ. TCF4, schizophrenia, and Pitt-Hopkins Syndrome. Schizophr Bull. 2010;36:443–7.
23. Thaxton C, Kloth AD, Clark EP, Moy SS, Chitwood RA, Philpot BD. Common pathophysiology in multiple mouse models of Pitt-Hopkins Syndrome. J Neurosci. 2018;38:918–36.
24. Wang Y, Lu Z, Zhang Y, Cai Y, Yun D, Tang T, et al. Transcription factor 4 safeguards hippocampal dentate gyrus development by regulating neural progenitor migration. Cereb Cortex. 2020;30:3102–15.
25. Gorski JA, Talley T, Qiu M, Puelles L, Rubenstein JL, Jones KR. Cortical excitatory neurons and glia, but not GABAergic neurons, are produced in the Emx1-expressing lineage. J Neurosci. 2002;22:6309–14.
26. Joshi PS, Molyneaux BJ, Feng L, Xie X, Macklis JD, Gan L. Bhlhb5 regulates the postmitotic acquisition of area identities in layers II-V of the developing neocortex. Neuron. 2008;60:258–72.
27. Dominguez MH, Ayoub AE, Rakic P. POU-III transcription factors (Brn1, Brn2, and Oct6) influence neurogenesis, molecular identity, and migratory destination of upper-layer cells of the cerebral cortex. Cereb Cortex. 2013;23:2632–43.
28. Lodato S, Rouaux C, Quast KB, Jantrachotechatchawan C, Studer M, Hensch TK, et al. Excitatory projection neuron subtypes control the distribution of local inhibitory interneurons in the cerebral cortex. Neuron. 2011;69:763–79.
29. Waite A, Brown SC, Blake DJ. The dystrophin-glycoprotein complex in brain development and disease. Trends Neurosci. 2012;35:487–96.
30. Miyoshi G, Fishell G. Dynamic FoxG1 expression coordinates the integration of multipolar pyramidal neuron precursors into the cortical plate. Neuron. 2012;74:1045–58.
31. Rannals MD, Hamersky GR, Page SC, Campbell MN, Briley A, Gallo RA, et al. Psychiatric risk gene transcription factor 4 regulates intrinsic excitability of prefrontal neurons via repression of SCN10a and KCNQ1. Neuron. 2016;90:43–55.
32. Seiradake E, del Toro D, Nagel D, Cop F, Härtl R, Ruff T, et al. FLRT structure: balancing repulsion and cell adhesion in cortical and vascular development. Neuron. 2014;84:370–85.
33. Liu YJ, Le Berre M, Lautenschlaeger F, Maiuri P, Callan-Jones A, Heuzé M, et al. Confinement and low adhesion induce fast amoeboid migration of slow mesenchymal cells. Cell. 2015;160:659–72.
34. Tachikawa K, Sasaki S, Maeda T, Nakajima K. Identification of molecules preferentially expressed beneath the marginal zone in the developing cerebral cortex. Neurosci Res. 2008;60:135–46.
35. De la Rossa A, Bellone C, Golding B, Vitali I, Moss J, Toni N, et al. In vivo reprogramming of circuit connectivity in postmitotic neocortical neurons. Nat Neurosci. 2013;16:193–200.
36. Hoy JL, Niell CM. Layer-specific refinement of visual cortex function after eye opening in the awake mouse. J Neurosci. 2015;35:3370–83.
37. Lanjakornsiripan D, Pior BJ, Kawaguchi D, Furutachi S, Tahara T, Katsuyama Y, et al. Layer-specific morphological and molecular differences in neocortical astrocytes and their dependence on neuronal layers. Nat Commun. 2018;9:1623.
38. Gordon JA, Stryker MP. Experience-dependent plasticity of binocular responses in the primary visual cortex of the mouse. J Neurosci. 1996;16:3274–86.
39. Crowley JC, Katz LC. Ocular dominance development revisited. Curr Opin Neurobiol. 2002;12:104–9.
40. Cappello S, Böhringer C, Bergami M, Conzelmann K-K, Ghanem A, Tomassy G, et al. A radial glia-specific role of rhoa in double cortex formation. Neuron. 2012;73:911–24.
41. Tsutsui KI, Witter MP. Entorhinal layer II calbindin-expressing neurons originate widespread telencephalic and intrinsic projections. Front Syst Neurosci. 2019;13:54.
42. Kitamura T, Pignatelli M, Suh J, Kohara K, Yoshiki A, Abe K, et al. Island cells control temporal association memory. Science. 2014;343:896–901.
43. Sekine K, Kubo K, Nakajima K. How does Reelin control neuronal migration and layer formation in the developing mammalian neocortex. Neurosci Res. 2014;86:50–58.
44. Rice DS, Curran T. Role of the reelin signaling pathway in central nervous system development. Annu Rev Neurosci. 2001;24:1005–39.
45. Hirota Y, Nakajima K. Control of neuronal migration and aggregation by reelin signaling in the developing cerebral cortex. Front Cell Dev Biol. 2017;5:40.
46. Hong SE, Shugart YY, Huang DT, Shahwan SA, Grant PE, Hourihane JO, et al. Autosomal recessive lissencephaly with cerebellar hypoplasia is associated with human RELN mutations. Nat Genet. 2000;26:93–96.
47. Zaki M, Shehab M, El-Aleem AA, Abdel-Salam G, Koeller HB, Ilkin Y, et al. Identification of a novel recessive RELN mutation using a homozygous balanced reciprocal translocation. Am J Med Genet A. 2007;143A:939–44.
48. Pankov R, Yamada KM. Fibronectin at a glance. J Cell Sci. 2002;115:3861–3.
49. Douezan S, Brochard-Wyart F. Active diffusion-limited aggregation of cells. Soft Matter. 2012;8:784–8.
50. Balaskas N, Abbott LF, Jessell TM, Ng D. Positional strategies for connection specificity and synaptic organization in spinal sensory-motor circuits. Neuron. 2019;102:1143–.e4.
51. Stoner R, Chow ML, Boyle MP, Sunkin SM, Mouton PR, Roy S, et al. Patches of disorganization in the neocortex of children with autism. N Engl J Med. 2014;370:1209–19.
52. Tang T, Zhang Y, Wang Y, Cai Z, Lu Z, Li L, et al. HDAC1 and HDAC2 regulate intermediate progenitor positioning to safeguard neocortical development. Neuron. 2019;101:1117–.e5.
53. Zhang Q, Zhang Y, Wang C, Xu Z, Liang Q, An L, et al. The zinc finger transcription factor Sp9 is required for the development of striatopallidal projection neurons. Cell Rep. 2016;16:1431–44.

54. Xiao L, Priest MF, Nasenbeny J, Lu T, Kozorovitskiy Y. Biased oxytocinergic modulation of midbrain dopamine systems. Neuron. 2017;95:368–.e5.
55. Gu Y, Cang J. Binocular matching of thalamocortical and intracortical circuits in the mouse visual cortex. eLife. 2016;5:e22032.
56. Gu Y, Huang S, Chang MC, Worley P, Kirkwood A, Quinlan EM. Obligatory role for the immediate early gene NARP in critical period plasticity. Neuron. 2013;79:335–46.
57. Niell CM, Stryker MP. Highly selective receptive fields in mouse visual cortex. J Neurosci. 2008;28:7520–36.